Toward room-temperature thermochromism of VO2 by Nb doping: magnetic investigations

Shian Guan, Mélanie Souquet-Basiège, Olivier Toulemonde, Dominique Denux, Nicolas Penin, Manuel Gaudon, Aline Rougier

Toward room-temperature thermochromism of VO_2 by Nb doping : magnetic investigations

Guan S.[1], Souquet-Basiège M. [1], Toulemonde O. [1], Denux D. [1], Penin N. [1], Gaudon M. [1], Rougier A. [1]

[1] *CNRS, Univ. Bordeaux, ICMCB, UMR 5026, F-33600 Pessac, France*

ABSTRACT

Using a synthesis route based on carbon as the reducing agent mixed with Nb-doped V_2O_5 nanopowders, highly crystallized Nb-doped VO_2 (M) particles, with tunable content of niobium (Nb), are successfully prepared. The morphology and the crystalline structure are first studied in regard to synthesis parameters and chemical composition for various thermal treatment temperatures/durations and niobium doping concentrations. The second part of this paper is devoted to the control, in Nb-doped VO_2, of the phase transition temperature from monoclinic to rutile (M → R transition) versus the niobium doping concentration associated with thermochromic properties and different property changes characterized by differential scanning calorimetry and magnetic and electrical measurements. The niobium introduction allows the decrease of the thermochromic transition from 68 °C down to around room temperature for an effective Nb concentration of approximatively 6 mol % for the $V_{0.94}Nb_{0.06}O_{2\pm\delta}$ composition. A significant result is the decrease of both the hysteresis width as well as the phase transition amplitude supported by latent heat, magnetic behavior, and electrical transport versus niobium concentration. These phenomena are correlated to the breaking of the V–V pairing occurring in the monoclinic form when niobium ions are introduced. Finally, a deep interpretation of the Nb-doped VO_2 magnetic behavior is performed considering the impact of niobium concentration and crystallite sizes on the intensity of the Curie magnetic residue plus Van Vleck susceptibility in the low temperature form (M) and on the intensity of the Pauli magnetism of the high temperature form (R).

Shian Guan, Mélanie Souquet-Basiège, Olivier Toulemonde, Dominique Denux, Nicolas Penin, et al.. Toward room-temperature thermochromism of VO_2 by Nb doping : magnetic investigations. *Chemistry of Materials*, American Chemical Society, 2019, 31 (23), pp.9819-9830. ⟨10.1021/acs.chemmater.9b03906⟩. ⟨hal-02401952⟩

Introduction

As a promising candidate for smart windows, vanadium dioxide (VO2) has aroused great attention due to the reversible metal-to-insulator transition (MIT) at a critical temperature (Tc = 68 °C), accompanied by a dramatic change in the optical properties in the near-infrared region and structural transition from a high-temperature rutile phase (R) to a low-temperature monoclinic phase (M).(1,2) In VO2 (R), the vanadium atoms occupy the lattice point of the body-centered cubic structure and are located at the centers of the VO6 octahedra. During the phase transition (R → M) (in cooling mode), the vanadium atom moves along the V–V direction, resulting in the pairing and twisting of the V4+ ions along the edge-sharing octahedral chains with additionally a tilting of VO6 octahedral cages.(3,4) Meanwhile, the thermal, magnetic, and conductivity properties of VO2 also exhibit a drastic transition near Tc.(5) As one of the long-lasting issues hindering the practical application of VO2 in smart windows, decreasing Tc to room temperature has attracted great attention.

To tailor the T_c value, elemental doping is widely used as a conventional strategy, which involves the intentional incorporation of atoms or ions of suitable elements into the host lattice. Several studies(6−19) have focused on the doping strategy to decrease the VO_2 (M/R) transition temperature to nearer room temperature (RT). Based on the Mott model explanation, namely, the correlation of the electron–electron driven MIT, there are two doping strategies to increase the carrier concentration and so decrease the T_c temperature: one is to insert monovalent doping atoms, such as H^+,(6) Li^+, and Na^+,(7) and the other strategy is to substitute the V sites with high-valence elements, such as tungsten (W^{6+}),(8−12) molybdenum (Mo^{6+}),(13) and niobium (Nb^{5+}).(14−20) The doping element either occupies the interstitial sites or substitutes the lattice V atom sites; it leads to variations in both the electronic and atomic structure of VO_2. Usually the second strategy is more efficient, especially for the W dopant. As the most effective dopant, W has been attracting great attention during these past years,(8−12) and it is reported that the electrons of W atoms are injected into the V 3d valence bands causing the T_c reduction up to 20–26 °C per atom %.(8) Some recent articles indicated that niobium would be even more efficient than tungsten if a greater doping fraction of the Nb content could be incorporated by the most adequate synthesis process.(16) However, as far as we know, there has been only one report of a transition temperature less than 30 °C for Nb-doped VO_2 oxide.(17) Most studies reported that the minimum T_c is between 30 and 50 °C.(16,18−20) It is believed that there is still a lack of suitable synthesis methods for Nb-doped VO_2 which is able to guarantee the achievement of a sufficiently high Nb-doping content (3 atom %–5 atom %).

Malarde et al.(14) used a continuous hydrothermal flow synthesis (CHNF) process to synthesize VO_2 and Nb-doped VO_2 nanoparticles (NPs), with particle sizes in the range of 50–200 nm. Pulsed laser deposition (PLD)(15) and aerosol-assisted chemical vapor deposition (AACVD) methods(16) are also reported to directly grow Nb-doped VO_2 films. Considering the high cost, low scale of production, and/or complex equipment associated with these different strategies, a new chemical preparation method should be developed.

In our previous work,(21) a novel carbo-thermal method was proposed to prepare nano- and microscale VO_2 (M) particles. In this synthesis process, carbon plays the role of reducing agent to prepare nano-VO_2 powder from higher valence vanadium oxide (V_2O_5) previously prepared as an intermediate compound. The V_2O_5 powder is homemade through the polyol process,(22) in which the target atoms or ions can be doped into the vanadium precursor (e.g., vanadyl ethylene glycolate, shortened as VEG). In short, pure VO_2 particles are synthesized following the route of VEG → V_2O_5 → VO_2. Unlike other methods using the reductive atmosphere, such as NH_3,(23) N_2H_4,(24) or H_2 and CO (combustion process),(25) the carbo-reduction synthesis is quite safe and highly reproducible. It overcomes many disadvantages, which are common in other thermal reduction methods, such as rigid experimental conditions, impurity, and poor stability of products. Besides, the particle size of as-prepared VO_2 can be easily controlled via changing the annealing conditions (e.g., temperature and time). In addition, we earlier reported successful Ti^{4+} and Al^{3+} doping into VO_2 (M) using this method.(21) Unfortunately, T_c almost remained unchanged. Herein, Nb doping will be achieved by simply modifying the process starting from the preparation of Nb-doped VEG precursor from the direct introduction of soluble niobium precursor. In this paper, in the first part, the aim is to prepare pure Nb-doped VO_2 powders with controlled morphology (nanoparticles, NPs) providing perfect samples to investigate the doping effects from all several aspects, including the morphology, crystal distortion, thermal stability, heat capacity, resistivity, and magnetic susceptibility. For instance, to study the crystal distortion during the phase transition (M/R), the distances of V–V and V–O and the angle of V–O–V will be carefully determined.

Besides, in this work, the change of vanadium valence (+3, +4, +5) after Nb doping is investigated through

Shian Guan, Mélanie Souquet-Basiège, Olivier Toulemonde, Dominique Denux, Nicolas Penin, et al.. Toward room-temperature thermochromism of VO_2 by Nb doping : magnetic investigations. *Chemistry of Materials*, American Chemical Society, 2019, 31 (23), pp.9819-9830. ⟨10.1021/acs.chemmater.9b03906⟩. ⟨hal-02401952⟩

chemical and thermogravimetric analysis (i.e., ICP and TG), which is usually measured using X-ray photoelectron spectroscopy (XPS).(14−16)

For example, Malarde et al.(14) found that the Nb doping did not have any signification effect on the oxidation of VO_2 and Nb-doped VO_2 powders, and the samples showed the same V^{4+}/V^{5+} ratio. Whereas a significant change of this ratio was reported by Quesada-Cabrera et al.(26) or by Barron et al.,(15) upon Nb incorporation, resulting in an increase of V^{4+} ions in the doped VO_2 sample. In short, the effect of Nb doping on the V valence is still unclear, and further work is needed. This valence issue will be discussed in the second part of this paper.

VO_2 (M/R) undergoes a magnetic transition, which can be characterized by an abrupt decrease in susceptibility near the phase transition temperature. It is characterized by Pauli and Curie-like paramagnetic (PM) behaviors above and below the T_c. Through experimental and theoretical investigations on pure VO_2, Zhang et al.(27) concluded that the abrupt decrease in susceptibility is due to that the VO_2 sample enters the singlet state in which the two electrons from adjacent V^{4+} ions are paired into dimers, which are formed due to the spin exchange between electrons. However, the discussions were only based on undoped VO_2. The M/R transition mechanism of VO_2 can be better studied through the elemental doping;(12) namely, the relationship between the atomic structure and magnetic property could unveil the transition in a clearer way. Thus, in the third and last part, the impact of Nb doping on the magnetic properties is also carefully investigated for a better understanding of the phase transition.

Experimental section

Materials

Ammonium metavanadate (NH_4VO_3; 99.0%), ethylene glycol (EG, $C_2H_6O_2$), Soot (Carbon black, S. A. 75 m^2/g; bulk density: 80–120 g/L), and $NH_4NbC_4O_9$, were purchased from PROLABO, Sigma, and Aldrich Alta-Aesar, respectively. All the chemical reagents were used as obtained commercially without further purification.

Synthesis

Vanadyl ethylene glycolate (VEG) precursor was synthesized through a polyol process. For the Nb-doped VEG preparation, 125 mL of ethylene glycol (EG) solution contained 1.42 g of ammonium metavanadate (NH_4VO_3), and a certain amount of $NH_4NbC_4O_9$ (Nb/Nb + V = 0%, 5 atom %, 10 atom %, and 15 atom %) were heated at 160 °C for 2 h under refluxing conditions. The final product (Nb-VEG) was centrifuged, washed 3 times with ethanol, and dried overnight in an oven at 80 °C. Then Nb-V_2O_5 was prepared by heating the Nb-VEG precursor at 300 °C for 90 min in air. Finally, the as-prepared Nb-V_2O_5 was grinded with carbon in a mole ratio of 1:1. The mixture was further annealed at 700 °C for 15 h in a dynamic vacuum system (DVS), created by pumping during the whole annealing process to maintain a vacuum environment (~10^{-4} mbar). According to the doping content and synthesis conditions (temperature and time), sample names are listed in Table 1.

Table 1. Sample List of VO_2 and Nb-Doped VO_2 Synthesized under Different Conditions

	doping percentage		
sample	targeted	ICP	synthesis conditions
VO_2-700A	0 atom %	–	700 °C + 15 h
5%-NbVO_2-700A	5 atom %	2.43 atom %	700 °C + 15 h
10%-NbVO_2-700A	10 atom %	5.77 atom %	700 °C + 15 h
VO_2-700B	0 atom %	–	700 °C + 1 h
VO_2-1000A	0 atom %	–	1000 °C + 15 h

Nb-doped VO_2 powders were prepared from the corresponding Nb-doped VEG precursors, which were synthesized thanks to the stoichiometric addition of Nb precursor besides the NH_4VO_3 in polyol medium, respectively; the polyol suspension was heated to 160 °C on a hot plate under reflux; the doped precursor was then collected by centrifugation (stage 1). The coprecipitation occurring during the heating under reflux of the

Shian Guan, Mélanie Souquet-Basiège, Olivier Toulemonde, Dominique Denux, Nicolas Penin, et al.. Toward room-temperature thermochromism of VO_2 by Nb doping : magnetic investigations. *Chemistry of Materials*, American Chemical Society, 2019, 31 (23), pp.9819-9830. ⟨10.1021/acs.chemmater.9b03906⟩. ⟨hal-02401952⟩

polyol starting suspension was visually followed (Figure 1). The complete dissolution of the ammonium metavanate and/or niobium chloride at room temperature is not achieved, and the polyol allows a total dissolution of the raw salts around 130 °C during the temperature rise (in between 125 °C (photograph no. 1) and 135 °C (photograph no. 2); the dissolution is associated with a pale orange and hazy suspension to a clear solution with darker orange color. The precipitation of the Nb-doped VEG precursor then occurs at around 150 °C, this precipitation being visibly conjugated to a reduction of V^{5+} ions (shift from a reddish suspension (photograph no. 3), to a suspension of particles with very dark purple color (photography no. 4)). The doped precursors were then annealed at 300 °C for 90 min in air in order to prepare a nano-Nb-doped V_2O_5 oxide powder (second stage). After mixing with carbon black with a molar ratio of 1:1, the mixtures were both annealed in a dynamic vacuum system at 700 or 1000 °C for typically 15 h to prepare Nb-doped VO_2 powder with various crystal sizes.

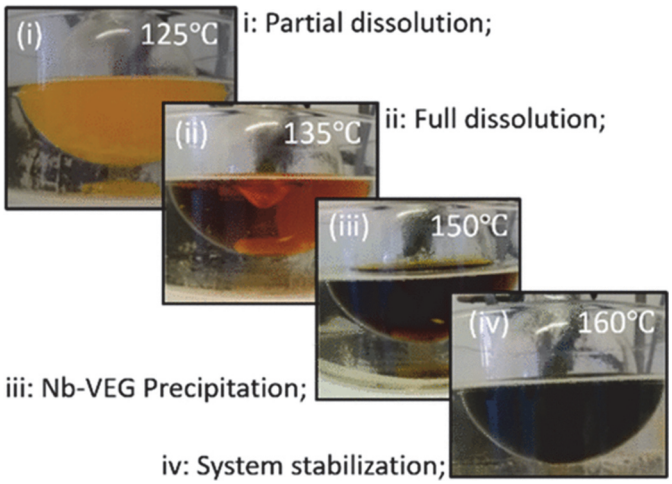

Figure 1. Photographs illustrating the different steps of the Nb-doped VEG precipitation.

Characterizations

The crystal structures of the as-prepared samples were determined by X-ray diffraction (XRD) analyses (Philips PW1820, PANalytical X' Pert PRO MPD diffractometer) performed using Cu $K\alpha_1$ radiation source (λ = 1.54056 Å), with the divergent slit of 1° and receiving slit size of 0.1 mm in a 2θ range from 8° to 80°. Moreover, Rietveld refinements were performed using FullProf software. The morphology of the as-prepared particles was observed by scanning electron microscopy (SEM) using JEOL JSM-6700F. The doping element content was determined in a 720-ES inductively coupled plasma–optical emission spectrometer (ICP-OES, Varian Inc.). The differential scanning calorimetry (DSC) experiment of VO_2 powders was performed using PerkinElmer DSC. In addition, the resistivity measurements were performed using Quantum Design X PPMS. Magnetic susceptibility was measured using both Vibrant MicroSense EZ7 and Quantum Design Magnetic Property Measurement System magnetometers. Data were collected in both ZFC and FC mode processes under an applied magnetic field of 1.5 T.

Results and discussions

Impact of the Niobium Doping on the Physicochemical Properties of the $V_{1-x}Nb_xO_{2\pm\delta}$ Oxide Powder

The crystallographic properties of the Nb-doped vanadium have been studied at the different stages of the synthesis route (i, precursor stage, the Nb-VEG precursor synthesis; ii, V^{5+} stage, Nb-V_2O_5 synthesis via the annealing Nb-VEG under air atmosphere; iii, V^{4+} stage, the carbo-thermal reduction to reach the Nb-doped VO_2). The effect of the insertion of Nb into the precursor structure is significant and associated with a clear amorphization: the diffraction peak of the precursor series for Nb concentration from 0% up to 15% (targeted concentration) continuously enlarges versus the concentration (Figure 2a). This is already a strong indication of the actual introduction of Nb ions into the bulk structure of the precipitated precursor. For the 15 mol %-doped VEG, the X-ray diffractogram no longer exhibits the characteristic peaks of the VEG precursor, but on the contrary, a single peak located on the 2-theta diffraction angle of 8.5° is observed (the origin of such diffraction peak cannot be clearly determined). Thus, the solubility limit (maximum content of niobium which can be incorporated into the VEG crystallographic network) seems to be reached between 10% and 15% in niobium.

Shian Guan, Mélanie Souquet-Basiège, Olivier Toulemonde, Dominique Denux, Nicolas Penin, et al.. Toward room-temperature thermochromism of VO_2 by Nb doping : magnetic investigations. *Chemistry of Materials*, American Chemical Society, 2019, 31 (23), pp.9819-9830. ⟨10.1021/acs.chemmater.9b03906⟩. ⟨hal-02401952⟩

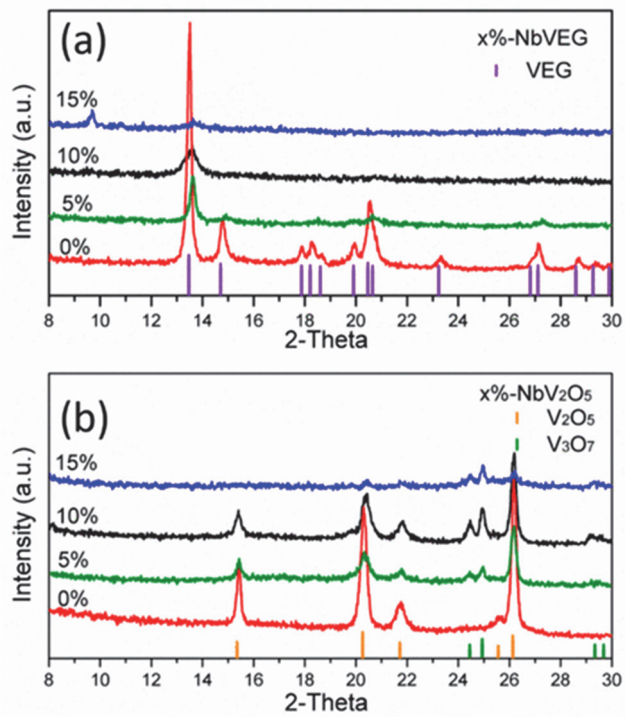

Figure 2. X-ray diffraction patterns of (a) the Nb-doped VEG precursor and (b) the nano-Nb-doped V2O5 for Nb target concentration ranging from 0 to 15 mol %.

After annealing at 300 °C for 90 min under air, a visible evolution of the crystallinity of the Nb doped powders with the Nb content is observed as represented by the diffractogramms in Figure 2b. As shown in some of our previous studies, the annealing of the undoped VEG leads to the obtention of pure V_2O_5 nanoparticles.(21,22) The Nb-doped V_2O_5 type phases resulting from air annealing of the Nb-doped VEG precursors are more amorphous: the width of the diffraction peaks enlarges with the increase in the Nb content. Moreover, while the Nb ions are incorporated, a "reducing" effect is observed: V_3O_7 oxide, corresponding to a mixed V^{4+}/V^{5+} oxidation states for vanadium ions, appears next to the V_2O_5 main phase for 5% and 10% Nb-doped samples; the V_3O_7 diffraction peak intensities increase versus the niobium concentration. The 15 mol % Nb-doped sample exhibits a diffractogramm corresponding to an almost amorphous sample (only some remaining small diffraction peaks can be indexed in the V_3O_7 phase). Thus, as observed for the Nb-doped VEG precursors, for the Nb-doped V_2O_5 samples obtained after a first annealing treatment under air, a drastic change is observed for target niobium concentration between 10 and 15 mol %. Subsequently, the following studies will only focus on the samples with a target niobium concentration in the range from 0 to 15%.

The Nb-doped V_2O_5 powders are then subjected to a carbo-thermal treatment according to the protocole developed previously in the laboratory to prepare undoped VO_2 compounds (stage 3).(21)Figure 3 displays the X-ray diffractograms of the series (with niobium target concentration from 0 to 15 mol %) issued from a similar carbo-thermal treatment (700 °C, 15 h), namely, the samples VO_2-700A and 5%-, 10%-, and 15%-NbVO_2-700A.

Shian Guan, Mélanie Souquet-Basiège, Olivier Toulemonde, Dominique Denux, Nicolas Penin, et al.. Toward room-temperature thermochromism of VO_2 by Nb doping : magnetic investigations. *Chemistry of Materials*, American Chemical Society, 2019, 31 (23), pp.9819-9830. ⟨10.1021/acs.chemmater.9b03906⟩. ⟨hal-02401952⟩

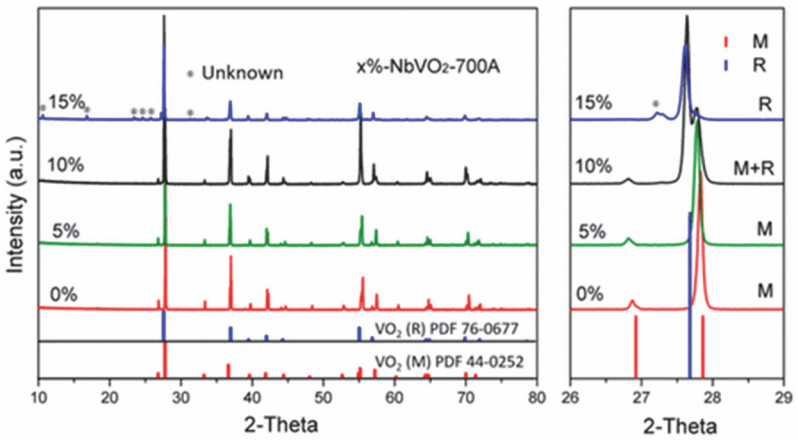

Figure 3. X-ray diffraction patterns of the Nb-doped VO2 powders obtained from carbo-thermal treatment for niobium concentration ranging from 0 to 15 mol %.

At first glance the similarities in the diffraction patterns of the VO_2-700A and 5%- and 10%-$NbVO_2$-700A compounds evidence that the effect of niobium introduction is far from obvious. Only the 15%-$NbVO_2$-700A exhibits a significantly different X-ray diffractogramm with the appearance of new peaks. However, a focus on the region of the (111) and (201) peaks indexed as from the VO_2 M monoclinic form, located respectively at 27° and 28°, and the (011) peak of the R rutile form (at about 27.5°), allows the rutile/monoclinic ratio to be determined, which increases greatly (rutile content increases whereas monoclinic content decreases) with the increase in the niobium concentration. Besides, the focus on this narrow angle domain (2θ between 26 and 29°) definitively shows that the 15%-$NbVO_2$-700A sample is not pure but contains some impurities, peaks well detected around 27.3° that do not correspond to the rutile or the monoclinic form.

In conclusion, the 0%-, 5%-, and 10%-$NbVO_2$-700A samples consist of the existence of the rutile and monoclinic phases (so these samples are with pure VO_2-type structures) of which proportion at room temperature is tunable from the niobium concentration.

The unit-cell parameters extracted from pattern matching of the rutile phase as well as the monoclinic phase when they are well detected in the X-ray powder patterns are reported in the Table 2.

Table 2. Unit-Cell Parameters of the *x*% Nb-Doped VO_2 Oxides for M and/or R Phases Extracted from Full-Pattern Matching

x%-$NbVO_2$-700A		*a* (Å)	*b* (Å)	*c* (Å)	*β* (deg)	unit-cell volume, *z* (Å^3)
0%	M	5.75225(4)	4.52591(4)	5.38301(5)	122.6088(5)	59.03
5%	M	5.76206(8)	4.52985(7)	5.38650(8)	122.6118(6)	59.22
10%	M	5.7699(2)	4.5358(2)	5.3898(2)	122.576(3)	59.43
	R	4.5602(2)	4.5602(2)	2.8651(6)	90	59.58
15%	R	4.5619(4)	4.5619(4)	2.8742(6)	90	59.82

The number of vanadium atoms in the VO_2 (M) unit cell is doubled as compared with those in the VO_2 (R) unit cell; here *z* is defined as 1 for VO_2 (R) and 2 for VO_2 (M). For the M phase, the unit-cell volume increases from 59.03 Å^3 to 59.22 Å^3 and 59.43 Å^3 after 5 atom % and 10 atom % doping, respectively. It should be mentioned that M and R phases coexist in the 10 atom % Nb-doped VO_2 sample (Figure 3b), and the unit-cell volume of the R phase shows a larger value of 59.58 Å^3 compared with the corresponding M phase form. When Nb doping content reaches 15 atom %, the R phase volume keeps increasing to 59.82 Å^3. The summarized evolution of the unit-cell volume, relative to the number of form units (V/z), increases linearly with the niobium concentration, following a Vegard law. Furthermore, knowing that the radius of Nb^{5+} (6-coordination number) is 0.64 Å, Nb^{4+} = 0.68 Å while V^{4+} = 0.58 Å, without presuming of the niobium oxidation state, the increase of the unit-cell parameters versus the niobium concentration is well expected.

At this point, chemical titration from ICP measurements was performed on the 5%- and 10%-$NbVO_2$-700A samples, i.e., for the two doped samples without any impurity detected by X-ray diffraction besides the VO_2 forms.

Shian Guan, Mélanie Souquet-Basiège, Olivier Toulemonde, Dominique Denux, Nicolas Penin, et al.. Toward room-temperature thermochromism of VO_2 by Nb doping : magnetic investigations. *Chemistry of Materials*, American Chemical Society, 2019, 31 (23), pp.9819-9830. ⟨10.1021/acs.chemmater.9b03906⟩. ⟨hal-02401952⟩

The effective concentrations of niobium ions in the pure Nb-doped VO_2 samples are 3 mol % (2.43 mol %) and 6 mol % (5.77 mol %) for the target concentrations of 5 and 10 mol %, respectively, i.e. for the 5%- and 10%-$NbVO_2$-700A samples. The precipitation efficiency of vanadium and niobium ions during coprecipitation is therefore different, and whatever the target concentration, the precipitation of the doping ions (niobium) gets a yield of about 60% only. This linear dependence between the target concentration (introduced in the polyol medium) and efficient concentration really introduces in the precipitate a good correlation evolution of the unit-cell parameters versus the target niobium concentration in Nb-doped VO_2 compounds that follow Vegard' law.

The SEM micrograph of the 10%-$NbVO_2$-700A illustrates the morphological evolution at the different synthesis stages (Figure 4a–c) (corresponding to the morphology of the 10%-Nb-doped VEG precursor, after stage 1; morphology of the 10%-Nb doped V_2O_5 intermediate compound, after stage 2; and the final morphology of the rutile/monoclinic VO_2 mixture, at the end of the synthesis process, stage 3). Considering in first approximation the particles as spherical objects, the particle size distribution widths for all three kinds of vanadium compounds obtained after the three synthesis stages are extracted from image treatment (Figure 4d).

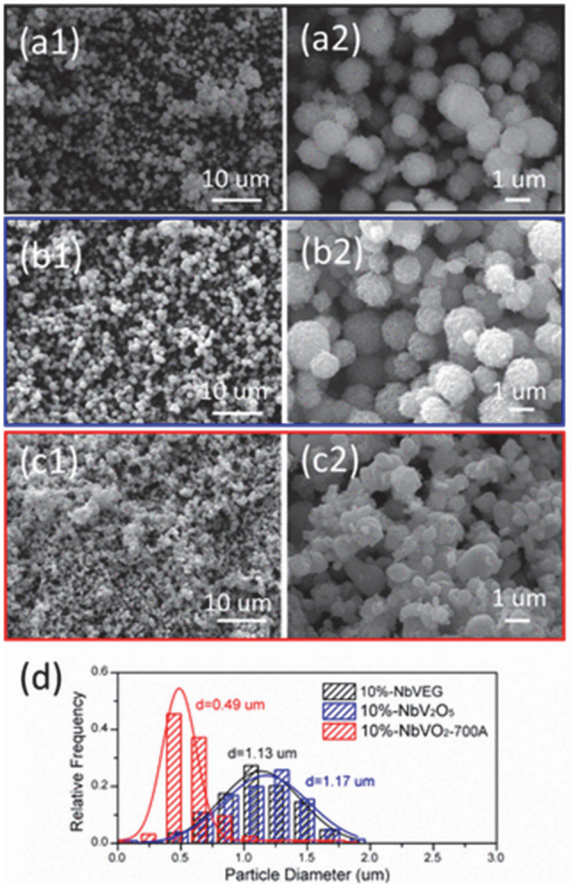

Figure 4. SEM images at two different magnitudes of (a1, a2) the 10% Nb-doped VEG precursor, (b1, b2) the 10% Nb-doped V2O5 intermediate compound, and (c1, c2) the 10% Nb-doped VO2 final compound (following the synthesis stages 1, 2, and 3, respectively) and (d) their corresponding particle size distributions.

The Nb-doped VEG precursor is very isotropic in shape; spherical particles of about a micrometer are observed with quite large distribution from 0.5 up to 1.75 μm around. Its morphology is quite different from the undoped VEG with an aggregation structure consisting of an elongated cuboid.(22) The Nb-doped V_2O_5 obtained after the intermediate air treatment exhibits similar morphology with exactly the same distribution width. This suggests that the VEG crystallites act like a template during the decomposition process of the organic part when the temperature increases. It has to be noticed that the spherical particles are now clearly polycrystalline: the spherical particle surfaces exhibit high roughness and can be described as strawberry-like aggregates of smaller crystallites. On the contrary, the high temperature treatment under vacuum destroyed this "preliminary" morphology while the oxides convert from V_2O_5 to VO_2. Quite isotropic but already faceted crystallites are observed for the as-prepared VO_2 monoclinic/rutile mixture, with a narrow distribution of size ranging from 0.4 to 0.8 μm. Aiming at deeper structural characterization, Rietveld analyses were performed. The monoclinic and rutile unit cells are

Shian Guan, Mélanie Souquet-Basiège, Olivier Toulemonde, Dominique Denux, Nicolas Penin, et al.. Toward room-temperature thermochromism of VO_2 by Nb doping : magnetic investigations. *Chemistry of Materials*, American Chemical Society, 2019, 31 (23), pp.9819-9830. ⟨10.1021/acs.chemmater.9b03906⟩. ⟨hal-02401952⟩

schematized in Figure 5a.

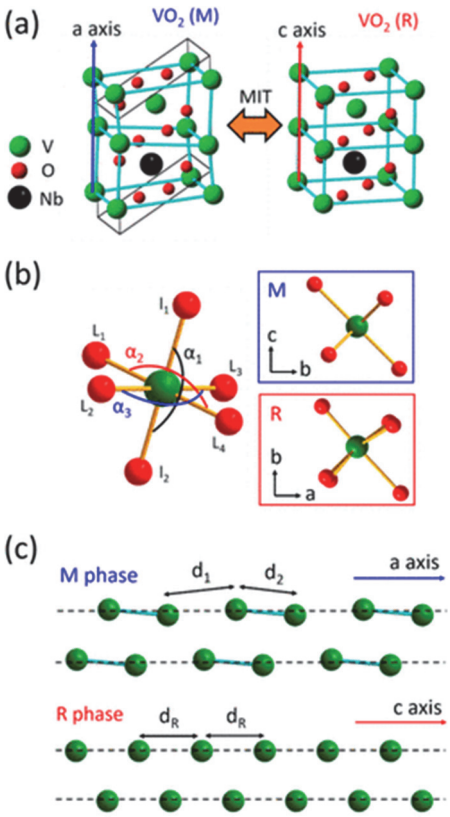

Figure 5. (a) Comparison of the monoclinic phase and rutile phase unit cells; (b) [VO6] octahedron unit full description in terms of bond lengths and bond angles; and (c) (V4+ ion) metallic-center position along edge-sharing octahedral chains (illustration of zigzag chain of the M phase and straight chain in the R phase).

The number of vanadium atoms in the VO_2 (M) unit cell is 12, which is double the 6 atoms for the VO_2 (R) unit cell. Upon R to M transformation, two main additional distortions can be isolated and discussed separately:

(i) The octahedral site distortion of the [VO_6] pattern unit is larger in M phase than in R phase. The vanadium atoms occupy the lattice point of the body-centered cubic structure and are located at the centers of the titled VO_6 octahedra. Two of the six oxygen atoms in the VO_6 octahedra are located further to the vanadium atom with a V–O bond distance of 1.93 Å (L bond length), while the other two oxygen atoms are located closer, and the V–O bond distances are 1.92 Å (l bond length). In VO_2 (M), due to the movement of vanadium atoms along the V–V direction, there is a slight change for the six V–O bond distances (L_1, L_2, L_3, L_4, l_1, and l_2 are different). Besides, the three angles of V–O–V (α_1, α_2, and α_3) are 180° in the R phase whereas these three angles can independently vary with significant amplitude from 180° in the M phase (Figure 5b).

(ii) The vanadium cation subnetwork is more distorted in the M phase than in R phase. The vanadium atoms move along the V–V direction (axis of the edge-sharing octahedral chains), and four different twins can form. Thus, the most apparent difference between the M and the R phase lies in the lengths of the V–V bonds, as illustrated in Figure 5c. In the M phase, the V^{4+} ions distribute periodically in a zigzag along the a_M axis, while in the R phase, a straight chain along the c_R axis is usually formed.

The V–V distances are constant in the R phase but alternatively varying within the M phase: the dimerization results in two different V–V bond lengths, a longer interdimer length (d_1) and a short intradimer length (d_2), in contrast to equally spaced V–V bonds (d_R) as in the R phase.

The distortion of the octahedral sites in monoclinic form in comparison with the octahedral site in rutile form, as reference, remains similar whatever the niobium content (Table 3). For different levels of Nb doping (0%, 5%, and 10%), the length change of V–O bonds in apical and equatorial directions shows similar distortion between the M and the R phase. Around 10.02% difference ($\Delta l/l_R$) is observed in the apical direction for these VO_2 samples.

Meanwhile, about 9.3% difference ($\Delta L/L_R$) is calculated in the equatorial direction. Regarding the angle distortion of V–O–V between the M and the R phase, a similar difference is displayed ($\Delta\alpha/\alpha_R$) with a value of 9.68% for different Nb dopings. In other word, the niobium to vanadium substitution has negligible impact on the octahedral site symmetry.

Table 3. From the Atomic Position Extracted by Rietveld Refinements on the Monoclinic Forms: V−O Bond Lengths and V−O Bond Angles Distance in the M Phase for 0%-, 5%-, and 10% Nb-Doped VO_2 Samples and Quantitative Assessment of the Octahedral Site Distortion in Comparison to the Octahedral Site of the R Phase

			0% ref R phase	0% M phase	5% M phase	10% M phase
V−O length (Å)	apical	l_1	1.9330	2.0489	2.0116	2.0245
		l_2	1.9330	1.7579	1.7760	1.7551
	length change (M/R_{ref})	$\Delta l/l_R$	0	10.86%	9.08%	10.13%
	equatorial	L_1	1.9216	1.8459	2.0503	2.0315
		L_2	1.9216	2.0240	1.9078	1.9397
		L_3	1.9216	2.0626	1.8637	1.8941
		L_4	1.9216	1.8726	2.0210	2.0428
	length change (M/R_{ref})	$\Delta L/L_R$	0	10.21%	9.01%	8.68%
V−O−V angle (deg)		α_1	180	171.482	171.451	172.624
		α_2	180	169.556	169.678	169.226
		α_3	180	168.453	168.954	168.884
	angle change (M/R_{ref})	$\Delta\alpha/\alpha_R$	0	9.86%	9.65%	9.53%

On the contrary, as gathered in Table 4, the longer V–V length (d_1) decreases while the shorter V–V length (d_2) increases versus the niobium introduction in monoclinic form. In other word, the ratio of d_1/d_2 shows a clear decreasing trend, and the ratio decreases from 1.205 to 1.194 and 1.160 after 5% and 10% Nb doping. In comparison, the ratio is 1 in the R phase. Besides, the distortions between M and R phases are also carefully studied: the distortion can be defined and calculated by using the $\Delta d = [(d_1 - d_R)^2 + (d_2 - d_R)^2]^{0.5}$ relation, where d_R is the V–V distance in the R phase (d_R = 2.8583 Å), as reference, arbitrarily fixed whatever the composition. Thus, the structural mismatches between the M and R phases decrease on the point of view of the spatial ordering of the cationic subnetwork. For the pure VO_2, the Δd distortion shows a quite high value of 0.3855 Å and decreases linearly with doping. In the range of 0% to 10% Nb doping, the decrease of $\Delta d/d_R$ from 13.51% to 12.88% and 10.94% indicates the decrease of the mismatch between the R and M phases. It further helps to interpret the impact of the Nb doping on both the transition temperature and the amplitude of the change in calorimetric, electrical, and magnetic properties.

Table 4. V−V Distance in the M Phase for the 0%, 5%, and 10% Nb-Doped VO_2 Samples and the V−V Pairing Distortion (Considering Zero or No Pairing Amplitude for the R Phase)

sample	phase	d_1 (Å)	d_2 (Å)	d_1/d_2	$R_{ref} \rightarrow M$; $\Delta d = [(d_1 - d_R)^2 + (d_2 - d_R)^2]^{0.5}$	$\Delta d/d_R$
0%	M	3.1632	2.6242	1.205	0.3855	13.51%
5%	M	3.1523	2.6399	1.194	0.3675	12.88%
10%	M	3.1181	2.6885	1.160	0.3121	10.94%
$0\%_{ref}$	R	2.8528	2.8528	1.000	0	0

The influence of the doping on the V–V distance is clearly shown, especially for the short distance (d_2), which determined the formation of the dimer. This distance slightly increases from 2.6242 to 2.6885 Å after 10% Nb doping. According to Coulomb's law, the longer vanadium atom distance indicates a weaker Coulomb interaction in the M phase. The weaker interaction of V–V in the dimer leads to an easier transition from the M to the R phase and further decreases the transition temperature from 68 to 25 °C after 10% Nb doping.

Shian Guan, Mélanie Souquet-Basiège, Olivier Toulemonde, Dominique Denux, Nicolas Penin, et al.. Toward room-temperature thermochromism of VO_2 by Nb doping : magnetic investigations. *Chemistry of Materials*, American Chemical Society, 2019, 31 (23), pp.9819-9830. ⟨10.1021/acs.chemmater.9b03906⟩. ⟨hal-02401952⟩

Thermochromic Transition: Comparison of the 0% and 10% Nb-Doped VO_2 Samples (VO_2-700A and 10%-$NbVO_2$-700A)

The 10%-$NbVO_2$-700A sample exhibits pure VO_2 type structure on the contrary to the 15% doped sample. Moreover, the 10% sample corresponds to an equilibrated mixture of the monoclinic and rutile phases at room temperature, indicating the transition temperature (T_c) could be probably decreased to room temperature. On a room temperature application point of view, the 10%-$NbVO_2$-700A sample appears the most promising. Rietveld refinement of the diffractogramm allows the calculation of the weight percent of monoclinic and rutile phases (Figure 6). At room temperature 10%-$NbVO_2$-700A consists of 54 wt % of the monoclinic form and 46 wt % of the rutile one (inset Figure 6). So, the coexistence of nearly 50% of each VO_2 phase proves that the phase transition is really calibrated near the room temperature and is expected to open a use on a large scale of such a compound as thermochromic film for smart windows. That is why we decided to investigate in the following discussion the difference in terms of calorimetric, electrical, and magnetic properties.

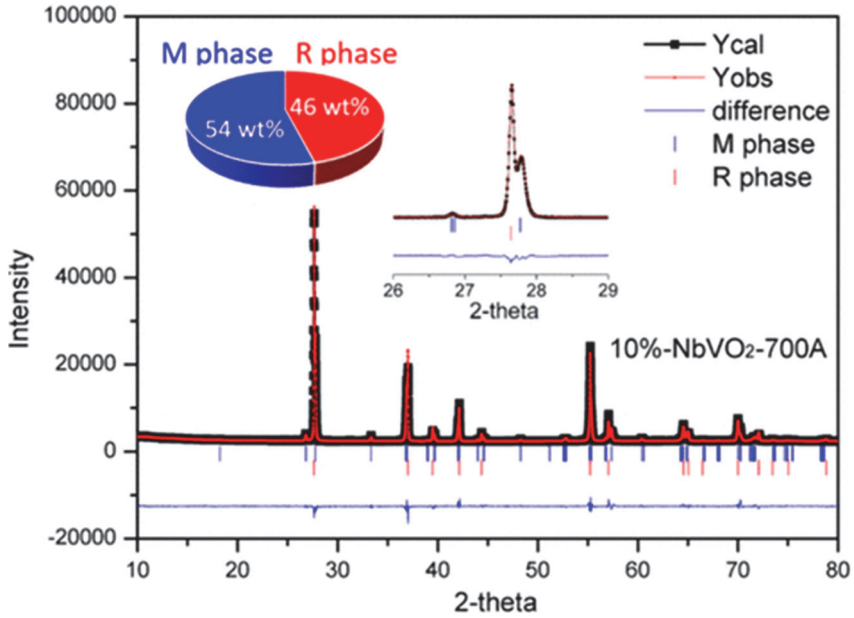

Figure 6. X-ray diffraction pattern refinement of the 10%-NbVO2-700A and extracted quantities for the VO2 (R) and VO2 (M) forms.

In order to get an idea of the oxidation state of both vanadium and niobium cations into the as-prepared 10%-$NbVO_2$-700A powder, TGA analyses were conducted on the undoped VO_2-700A powder under air aiming at producing the full oxidation of V^{4+} into V^{5+} cations (Figure 7).

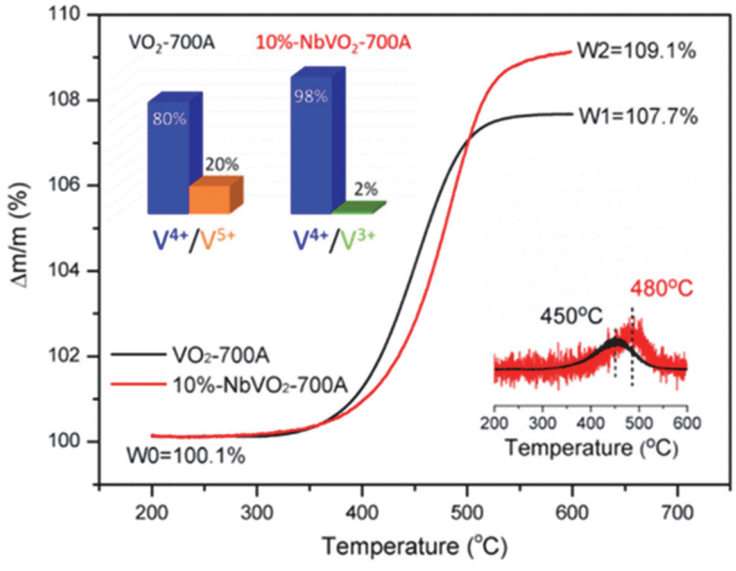

Shian Guan, Mélanie Souquet-Basiège, Olivier Toulemonde, Dominique Denux, Nicolas Penin, et al.. Toward room-temperature thermochromism of VO_2 by Nb doping : magnetic investigations. *Chemistry of Materials*, American Chemical Society, 2019, 31 (23), pp.9819-9830. ⟨10.1021/acs.chemmater.9b03906⟩. ⟨hal-02401952⟩

Figure 7. TGA analyses under air atmosphere performed on the 10%-NbVO2-700A and the VO2-700A samples. Molar proportion of V3+/V4+ and V4+/V5+ in both cases.

After the high temperature (600 °C) TGA experiment, the powder color changes to orange, which is a typical V^{5+} color suggesting a full transformation to V_2O_5. With Nb doping, there is a slight improvement in thermal stability, and the oxidation temperature increases from 450 to 480 °C. For the undoped sample, the chemical formula changed from $VO_{2\pm\delta}$ to $VO_{2.5}$ during the TGA, and the mass variation associated with the oxidation leads to calculating a $\delta = 0.1$ and further a V^{4+}/V^{5+} content ratio equal to 4 (80 mol %/20 mol %). This result is in agreement with literature studies where it has been proved that V^{4+} and V^{5+} usually coexist in undoped VO_2;(6,14,15) even if a pure VO_2 crystal is obtained, it can be reasonably assumed that surface oxygen overstoichiometry leads to the occurrence of a significant proportion of V^{5+} ions. For the 10%-$NbVO_2$-700A sample, we consider the starting chemical formula $V_{1-x}Nb_xO_{2\pm\delta}$ with the x value issued from the ICP titration equal to 5.77 atom % and without presuming of the oxidation state of vanadium. In order to extract the vanadium average oxidation state, Nb is assumed to have an oxidation state +5, i.e., without any trace of Nb with an oxidation state equal +4. With this hypothesis, the vanadium oxidation state is found to be 3.95, meaning nearly with all the vanadium ions (98 mol %, exactly) with a +4 oxidation state but also with traces of +3 vanadium (2 mol %); this is coherent with a compensation of the aliovalent substitution of the V^{4+} from the Nb^{5+}. Indeed, the electroneutrality law engages the reduction of vanadium ions in order to compensate this aliovalent substitution. Hence, it can be concluded that in doped or undoped samples the largest quantity of vanadium species exhibits a +4 oxidation state. Also, TGA under an oxidation atmosphere seems coherent with the consideration of a +5 oxidation state for the niobium doping ion.

To further investigate the influence of the vanadium to niobium substitution on the first order transition of VO_2 (M/R), differential scanning calorimetry (DSC), resistivity, and vibrating-sample magnetometer (VSM) in situ measurements versus temperatures were performed. As shown in Figure 8a–c, a sudden transition occurs in both samples. The heat capacity, resistivity, and magnetic susceptibility temperature dependences show for both samples a first-order transition exhibiting a clear hysteresis loop in between the heating and the cooling processes. The transition temperatures (T_c) in the heating and cooling cycle for the undoped and the 10%-Nb-doped VO_2 samples are gathered in Figure 8d.

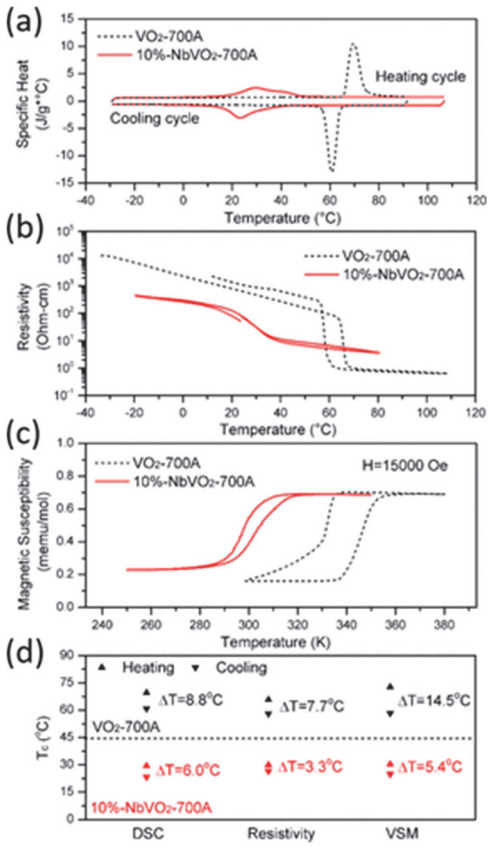

Figure 8. (a) DSC curves showing the heat capacity, (b) resistivity curve, and (c) magnetic susceptibility of VO2 (VO2-

Shian Guan, Mélanie Souquet-Basiège, Olivier Toulemonde, Dominique Denux, Nicolas Penin, et al.. Toward room-temperature thermochromism of VO_2 by Nb doping : magnetic investigations. *Chemistry of Materials*, American Chemical Society, 2019, 31 (23), pp.9819-9830. ⟨10.1021/acs.chemmater.9b03906⟩. ⟨hal-02401952⟩

700A) and Nb-doped VO2 (10%-NbVO2-700A) versus temperature. (d) Summary of transition temperatures and the width of the hysteresis loop measured between heating and cooling modes extracted from DSC, resistivity, and VSM analyses.

From pure VO_2, the T_c around 70 °C greatly decreases to 25 °C after Nb doping, being in good agreement with the occurrence of a monoclinic/rutile mixture at room temperature as analyzed previously from X-ray diffraction pattern refinement. The widths of the hysteresis loop associated with this first order transition associated to the temperature mismatch in between the heating and the cooling cycles measured by the different techniques show a narrower transition width with Nb doping. On one hand, the impact on the transition temperature of doping ions inside VO_2 structures (as for Nb^{5+} ion doping) is intensively studied and discussed in the literature, even if it remains the subject of controversy.(28,29)

On the other hand, and more interestingly, the niobium doping is associated with a decrease of the hysteresis width as well as a decrease of the latent heat on the transition and a decrease of the amplitude mismatch in terms of electrical conductivity and magnetization values. For illustration, for the 10%-$NbVO_2$-700A, the latent heat as measured in the heating cycle is 33.42 J/g and, in the cooling cycle, is 33.39 J/g, which is expected to result from the combined contributions of the phonons and electrons coexisting within the phase transition.(30) The latent heat ratio 33.42/33.39 = 1.001 clearly demonstrates that the transition is perfectly reversible, while as a comparison, the latent heat of the undoped VO_2 is 54.26 and 53.61 J/g in the heating and cooling cycles, respectively, which also displays an excellent reversibility with a latent heat ratio of 54.26/53.61 = 1.012. This is in good agreement with a smaller hysteresis in the case of Nb doped VO_2. Indeed, the latent heat and hysteresis width reductions are both linked to a decrease of the energetic barrier to cross through the first order phase transition, which can be put in regard to the structural mismatch between R and M phases versus doping.

More spectacularly, a deeper investigation was conducted on the electrical conductivity (σ) versus temperatures (on heating mode) of both undoped and doped samples (Figure 9). As the temperature increases, there is a sharp transition for both samples. The conductivity of the semiconducting state (low temperature) is enhanced significantly by the Nb substitution, while the one of the metallic state (high temperature) is reduced. The monoclinic pellet exhibits a semiconductor behavior, while the rutile pellet, reported to display a metallic behavior, shows here also a semiconducting behavior with a higher conductivity.(5) The thermally activated conductivity exhibits the Arrhenius dependence, and ln σ is a linear function of $1000/T$ in both sides of the transition from the function $\sigma = \sigma_0 \exp(E_a/kT)$. The high R^2 value shows an excellent fitting. Assuming then that the slope is directly linked to the band gap, the "activation energy" (E_a) can be calculated for both monoclinic and rutile forms for both samples. The calculated E_a is shown in the inset of Figure 9. For the VO_2-700A sample, E_a is 0.387 and 0.113 eV for its monoclinic and rutile phase, and the corresponding E_a values are 0.256 and 0.202 eV for the 10%-$NbVO_2$-700A sample. Clearly, in terms of activation energies, the mismatch between two phases is nearly suppressed as Nb substitution is introduced into the VO_2 lattice. It is expected that the breaking of Peierls distortion and the weakening of electronic correlation within the V–V dimers would result in a decrease of the band gap (for M phase), leading to the decrease in T_c and increase of σ in the low temperature. Here the local V–V dimer distance, and especially the pairing strength, characterized previously as described in XRD part from the ratio between the long V–V length and the short V–V length (d_1/d_2), is slightly decreased from 1.205 for the undoped sample to 1.16 after 10% Nb doping; hence, it facilitates thermal activation of carriers and, so, the monoclinic to rutile phase transition.

Shian Guan, Mélanie Souquet-Basiège, Olivier Toulemonde, Dominique Denux, Nicolas Penin, et al.. Toward room-temperature thermochromism of VO_2 by Nb doping : magnetic investigations. *Chemistry of Materials*, American Chemical Society, 2019, 31 (23), pp.9819-9830. ⟨10.1021/acs.chemmater.9b03906⟩. ⟨hal-02401952⟩

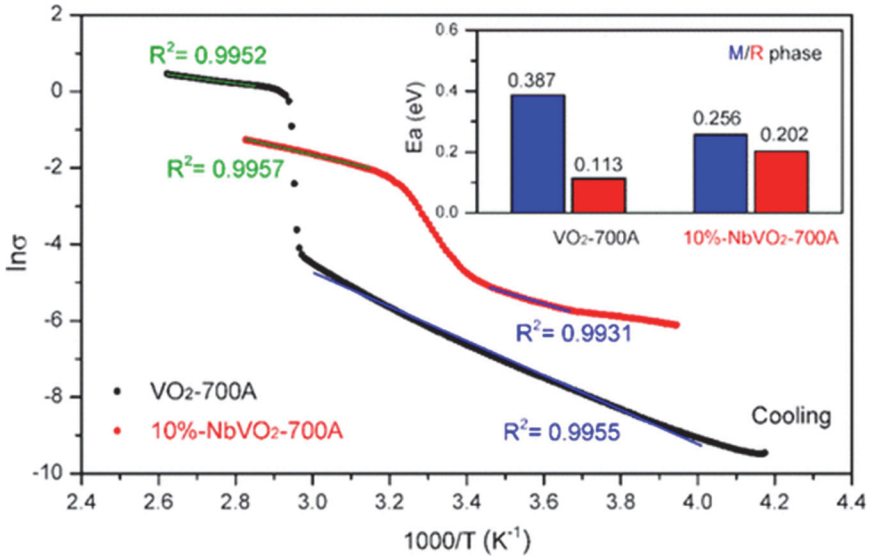

Figure 9. Detailed study on the temperature dependence of the conductivity of undoped and Nb-doped VO2 samples (VO2-700A and 10%-NbVO2-700A) along the phase transition, with large R2 showing good fitting; the activation energies (Ea) for both M and R forms are inserted.

Single crystals of VO_2 typically yield an E_a of 0.45 eV, and doping with a valence greater than +4 will sharply lower this value. For example, the E_a of the M phase is decreased to 0.22 eV for W^{5+} doping and 0.1 eV for Mo^{6+} doping with a content of around 0.05–0.5 atom %.(31) In fact, it is also reported that the E_a would be lowered after Al^{3+} doping.(32) Unexpectedly, above T_c, the electrical behavior of the Nb-doped sample is not a metal. It seems that both R and M phases are both a semiconducting phase, suggesting the electronic nature of the transition is different from the classic Mott metal–insulator transition,(33) or rather that the electronic conductivity is limited by the grain boundary conductivity.

All these observations converge toward a decrease of the mismatch between the M and the R phases. This phenomenon is to be correlated to the previous discussions issued from our Rietveld analyses that have shown an accommodation of the structural transition while niobium is introduced in the crystallographic VO_2 network (accommodation which is due to the partial "de-pairing" of the V entities in dimers while Nb doping). Clearly, it reveals a correlation between the distortion of the V–V pairing caused by niobium doping and the decrease of the latent heat, the resistivity, and the magnetization mismatches along the transition. It has to be noted that the latent heat is already known as to be made up from the accumulation of two contributions;(5) one is from the lattice which results from the crystalline distortion and the other one from the conduction electrons which results from the discontinuity in the carrier density. Our study shows that the decrease of the conductivity mismatch in between the R and M phases as well as the decrease of the crystallographic mismatch associated to the M and R transition are closely related; thus, structural considerations and electrical and magnetic properties through the phase transition seem actually entangled.

Deeper Investigation of the Magnetic Properties: Impact of Doping Concentration and Particle Size

The last part of our study focuses on the magnetic properties and their comparison on five selected samples: the first three samples, VO_2-700A abd 5%- and 10%-$NbVO_2$-700A, allow a study of the impact of the niobium doping rate, between samples prepared using the same synthesis parameters; the sample VO_2-700A is to be compared with samples VO_2-700B and VO_2-1000A, and as for undoped samples the crystallite sizes vary thanks to different thermal treatments (the VO_2-700B sample is annealed only 1 h at 700 °C, while the VO_2-1000A sample is annealed 15 h at 1000 °C). SEM images of the three latter samples are reported in Figure 10. The average crystallite sizes deduced from image treatments for the three samples are 0.4 µm for the VO_2-700B, 1.8 µm for the VO_2-700A, and 5.3 µm for the VO_2-1000A sample.

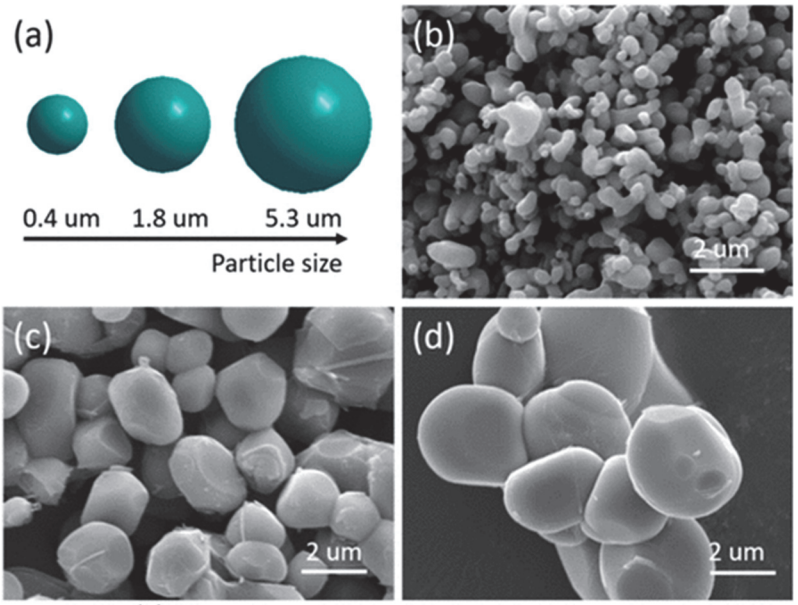

Figure 10. (a) Annealing temperature effect on VO2 particle size. SEM images of the (b) VO2-700B, (c) VO2-700A, and (d) VO2-1000A samples.

Figure 11 displays the magnetic susceptibility vs T curve measured in the field of 15 000 Oe during the cooling process for a wide range of temperatures from 380 K to 2 K with a SQUID magnetometer apparatus. For all five samples, a clear magnetic susceptibility drop can be clearly observed at the transition critical temperature T_c from rutile (high temperature) to the monoclinic (low temperature) form. The collected data can then be divided into high-T ($T > T_c$) and low-T range ($T < T_c$). Above T_c, the plateau with roughly constant susceptibility in high temperature is associated to Pauli paramagnetism (PM) in relation with the high electronic conductivity of the rutile form as just underlined. To explain the low-T susceptibility plateau, the formation of covalent V–V pairs was suggested.(34) After this stable value in the temperature range of 300–150 K, the magnetic susceptibility shows a rapid increase below 150 K, which was interpreted by the presence of traces of unpaired V^{4+} spins probably due to defaults (lattice defects) in the structure.(35)

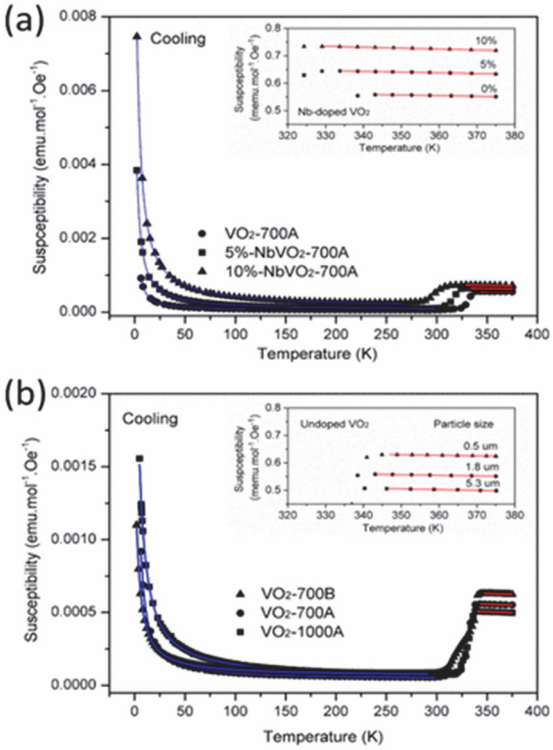

Figure 11. Susceptibility versus temperature of the (a) VO2-700A, 5%-NbVO2-700A, and 10% NbVO2-700A compounds and (b) VO2-700A, VO2-700B, and VO2-1000A compounds. Insets are the plots of the fits (red lines) performed on the

Shian Guan, Mélanie Souquet-Basiège, Olivier Toulemonde, Dominique Denux, Nicolas Penin, et al.. Toward room-temperature thermochromism of VO_2 by Nb doping : magnetic investigations. *Chemistry of Materials*, American Chemical Society, 2019, 31 (23), pp.9819-9830. ⟨10.1021/acs.chemmater.9b03906⟩. ⟨hal-02401952⟩

experimental susceptibilities in the high temperature domain.

First, we discuss the variation of the Pauli plateau values in the high-T range for different samples. The fits of the Pauli magnetic part were made by refining two key variables: the Fermi energy (E_F^0) of the compound and the number of charge carriers per mol (N_P) using the following equations,

$$\chi_P = \chi_P^0 \left[1 - \frac{\pi^2}{12}\left(\frac{k_B T}{E_F^0}\right)^2\right] \ldots \text{Pauli PM} \quad (1)$$

$$\chi_P^0 = N_P a \quad (2)$$

$$a = \frac{3\mu_B^2}{2E_F^0} \quad (3)$$

where k_B = 8.617 × 10^{-5} eV/K is the Boltzmann constant and μ_B = 5.788 × 10^{-5} eV/K-Bohr magneton.

The plots of the different fits are added to experimental data in the inset of Figure 11, and the different parameters calculated from the fits are gathered in Table 5. An ideal crystal of VO_2 should be diamagnetic if Van Vleck's orbital paramagnetism is neglected. Then below T_c, the low temperature parts of the susceptibility curves were also fitted considering in the monoclinic form the sum of (i) a Curie–Weiss law χ_{cw} due to traces of unpaired spins $\chi_{cw} = C/(T - \theta)$ and (ii) a temperature-independent paramagnetism (χ_{TIP}^0) consist of Van Vleck susceptibility and diamagnetic susceptibility to account for the magnetic susceptibility plateau. This interpretation of the low magnetic susceptibility is quite close from the one proposed by Wang et al.,(36) but using $\chi_{cw} = C/T$ leads here to significantly poorer reliability factors. Also, it can be noticed that they interpreted the absence of the magnetic moment associated to V–V pairs from spin pairing of the electrons from adjacent V^{4+} ions along the chain direction at an angle θ close to 180°, on the contrary to us. Other tests, by the same group,(27) led to the proposition of a spin gap system due to the V–V dimerization state with an antiferromagnetic interaction. The magnetic susceptibility would result from the thermal activation from singlet to triplet levels, but these considerations were unsuccessfully giving gap values in the range of 2 K which can be assumed irrelevant. The temperature independent paramagnetic contribution susceptibility, Curie constant (C), and Curie–Weiss temperature (θ) as well as correlation factors are reported in Table 6.

$$\chi = \chi_{TIP}^0 + \frac{C}{T - \theta} \ldots \text{Low } T^\circ \text{ PM} \quad (4)$$

From the so-obtained fitted parameters, the χ_{TIP}^0 susceptibility value is positive, meaning that the Van-Vleck's orbital paramagnetism cannot be neglected. Furthermore, it is more significantly impacted by the niobium substitution for vanadium than by crystallite sizes and/or surface defects. The Curie constant C increases significantly with the niobium concentration and/or with the increase of the average crystallite size of the analyzed sample. The Curie–Weiss temperatures θ remain near equal to zero whatever the sample, indicating weak strength between the magnetic species.

Shian Guan, Mélanie Souquet-Basiège, Olivier Toulemonde, Dominique Denux, Nicolas Penin, et al.. Toward room-temperature thermochromism of VO_2 by Nb doping : magnetic investigations. *Chemistry of Materials*, American Chemical Society, 2019, 31 (23), pp.9819-9830. ⟨10.1021/acs.chemmater.9b03906⟩. ⟨hal-02401952⟩

Table 5. Pauli Susceptibility (χ_P^0), Fermi Energy (E_F^0), Charge Carrier Concentration (N_P), and R^2 of the Fitting Results for the VO_2-700A, 5%-$NbVO_2$-700A, 10% $NbVO_2$-700A, VO_2-700B, and VO_2-1000A Compounds

	sample		χ_P^0 ($\times 10^{-5}$ emu·mol^{-1}·Oe^{1-})	E_F^0 (meV)	N_P ($\times 10^3$)	R^2
doping effect	VO_2-700A	0%	59.46 ± 0.11	108.79	12.9	0.9950
	5%-$NbVO_2$-700A	2.43%	71.80 ± 0.15	105.94	15.1	0.9935
	10%-$NbVO_2$-700A	5.77%	78.58 ± 0.18	101.33	15.8	0.9917
size effect	VO_2-700B	0.5 μm	66.41 ± 0.11	120.40	15.9	0.9874
	VO_2-700A	1.8 μm	59.46 ± 0.11	108.79	12.9	0.9950
	VO_2-1000A	5.3 μm	54.98 ± 0.16	96.06	10.5	0.9838

The impact of the niobium concentration on the χ_{TIP}^0 susceptibility can be expected from the different electronic configurations of the niobium ions and the vanadium ones, with a larger quantity of valence band electrons in niobium (the heavier atom) in comparison with vanadium (the lighter atom). Interestingly, the Van Vleck magnetic susceptibility has already been found to scale linearly with Nb dopant in $BaTiO_3$ diamagnetic matrices.(37) Our result suggests a possible counter charge balance introducing one V^{3+} for each Nb^{5+}.
The Curie constant exhibits for all the samples a very low value, confirming the d electron trapping into homopolar bonds in relation with the dimer formation of largely most of the vanadium (+4) ions in the monoclinic form, in good agreement with literature.(38) Hence, the reported Curie magnetism definitively has to be discussed as a "residual paramagnetism". This also explains why the Van Vleck magnetism is generally neglected in semiconducting oxide with paramagnetic atoms, because its relatively weak amplitude must be taken into account. More interesting is the variation of the Curie constant with crystallite size and Nb concentration.

Table 6. Van Vleck and Diamagnetic Susceptibility (χ_{TIP}^0), Curie Constant (C), Curie–Weiss Temperature (θ), and R^2 of the Fitting Results for the (i) VO_2-700A, 5%-$NbVO_2$-700A, 10% $NbVO_2$-700A, VO_2-700B, and VO_2-1000A Compounds

	sample		χ_{TIP}^0 ($\times 10^{-5}$ emu·mol^{-1}·Oe^{1-})	C (10^{-3})	θ	R^2
doping effect	VO_2-700A	0%	3.69 ± 0.03	4.91 ± 0.02	0.81 ± 0.02	0.99991
	5%-$NbVO_2$-700A	2.43%	7.16 ± 0.12	15.26 ± 0.07	−1.83 ± 0.02	0.99988
	10%-$NbVO_2$-700A	5.77%	9.91 ± 0.48	33.39 ± 0.30	−2.39 ± 0.04	0.99947
size effect	VO_2-700B	0.5 μm	6.00 ± 0.02	4.95 ± 0.01	−2.75 ± 0.02	0.99983
	VO_2-700A	1.8 μm	3.69 ± 0.03	4.91 ± 0.02	0.81 ± 0.02	0.99991
	VO_2-1000A	5.3 μm	4.10 ± 0.07	10.62 ± 0.06	−2.15 ± 0.05	0.99963

Reasonably, considering all the niobium ions with the +5 oxidation state, i.e., showing diamagnetic signal and a significant Van Vleck magnetic susceptibility, the Curie residual paramagnetic can only result from unpaired V^{4+} ions and/or vanadium ions with low oxidation state (+3) as previously suggested. Unpaired vanadium ions can be located at the end of a V–V dimerization along the chain, meaning at the crystal surface or in first-neighboring Nb^{5+} ions. Hence, it can well explain the increase of the Curie constant with defects as Nb^{5+} ions acting like "breaking points" along the chains formed by the edge-sharing octahedral sites. However, the increase of the Curie constant with the crystallite sizes appears illogical, on this point of view. Apparently, the predominant reason for this latter phenomenon is due to the occurrence of a small fraction of V^{3+} ions as it has been shown from TGA measurements (Figure 7). This V^{3+} fraction increase versus the thermal treatment temperature is expected since the temperature is always associated with a reductive effect. Finally, the constant value near 0 K for the Curie–Weiss temperatures can be interpreted in regard to the absence of long-range magnetic ordering between traces of unpaired V^{4+}.

As proposed by Goodenough,(34) in the rutile phase, a narrow π^* antibond is formed between the V^{4+} and O^{2-}, and a $d_{//}$ nonbond is formed between adjacent V^{4+} orbitals along the crystallographic c axis. The unfilled π^* and $d_{//}$ bands partially overlap, and the Fermi level (E_F^0) falls at the point where π^* and the $d_{//}$ bands overlap, as illustrated in Figure 12a. During the phase transition R → M, the π^* level is elevated and the $d_{//}$ bond is split into $d_{//}$-bonding and $d_{//}^*$ antibonding due to V–V dimers formation. Here the position of the E_F^0 with respect to valence and or conduction bands depends on various parameters such as the temperature, the effective masses of electrons, and the number of free electrons. For the undoped VO_2, the Fermi energy is lying exactly at the middle of the energy bandgap at T = 0 K. In order to maintain the number of particles (mass action law) and to fulfill the overall electrical charge neutrality (neutrality equation), the E_F^0 moves toward the conduction band when the Nb^{5+} (donor) is introduced, which gives additional electrons from the system. In our case, versus Nb doping

concentration and particle size increase, the E_F^0 displays a clear decreasing trend. Based on the SQUID measurement and the simulation, below T_c, the number of near-free electrons in R and M phases can be calculated by considering the previous eqs 1, 2, and 3 and additionally the new eq 5:

$$\chi_{TIP}^{0} = (N_p - 2N_{d0})a \qquad (5)$$

where Np is the number of near-free electrons in the R phase and Nd0 is the number of dimers in the M phase. Because each dimer contains two electrons, the number of near-free electrons would change from Np to (Np – 2Nd0) in the M phase and (Np – 2Nd0)/Np is the percentage of unpaired V4+ ions.(27) The results are presented in Figure 12b.

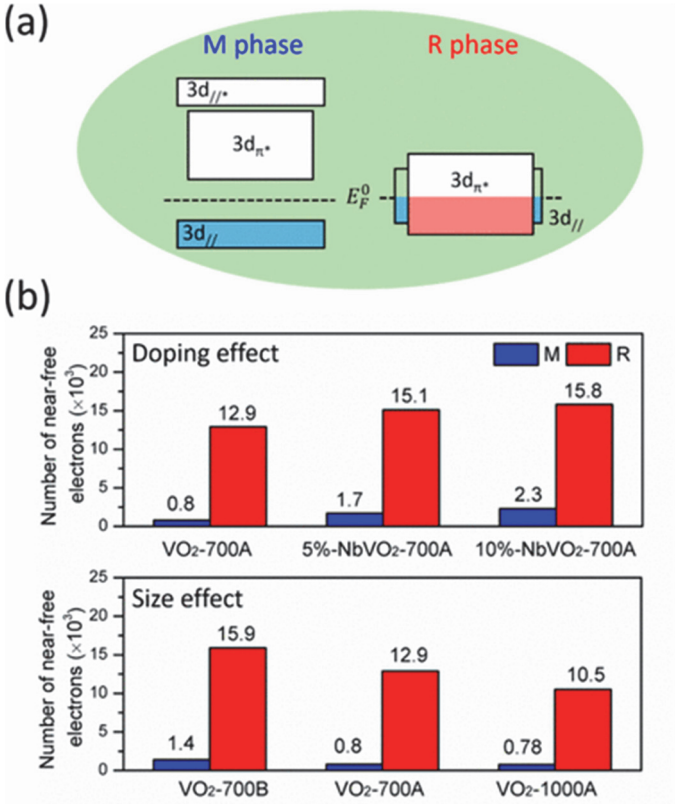

Figure 12. (a) Band structures of VO2 (M/R) depicted by molecular orbital diagrams; (b) number of near-free electrons in M and R phases: doping effect for the VO2-700A, 5%-NbVO2-700A, and 10% NbVO2-700A compounds and size effect for the VO2-700A, VO2-700B, and VO2-1000A compounds.

It can be seen that the major V^{4+} ions are paired into V–V dimers, and ~94% V^{4+} are paired into dimers for the undoped VO_2. Due to the breaking of Peierls distortion as Nb substitution, the unpaired "free" V^{4+} ions percentage increased from ~6% to ~11% and ~15%. As for particle size increases, the unpaired V^{4+} ions percentages are ~9%, ~6%, and ~7%, the size particle effect is not so clear. During the phase transition R → M, as previously pointed out the V ions are shifted to form V–V pairs. The V–V pairs may trap all the available d electrons into homopolar bonds as suggested by Goodenough.(34)

Conclusion

In this work, Nb-doped VO_2 particles were successfully synthesized using the carbo-thermal method. More precisely, the process can be described in three stages, namely, (i) Nb-VEG formation through the polyol process, (ii) oxidation to Nb–V_2O_5 in air annealing, and (iii) reduction to Nb-VO_2 due to carbon black addition. Thanks to this specific method, Nb content up to 5.77 atom % was nicely achieved leading to a decrease in the transition

temperature T_c, getting close to 25 °C. Hence, the phase transition was perfectly adjusted near room temperature, as expected for use as a thermochromic film for the next generation of smart windows. The influence of the Nb doping on the thermochromic properties of Nb-doped VO_2 was investigated by differential scanning calorimetry (DSC), resistivity measurements, and scarcely used vibrating-sample magnetometer (VSM) characterizations showing a strong dependency to the Nb content as well as the crystallite sizes. In particular, the input of the magnetic characterizations allows a significant step forward in the determination of the V/Nb cation distribution, bringing crucial information for further consideration in the remaining debates on the origin of the driving force(s) behind the metal–insulator transition (MIT) of VO_2.

Acknowledgements

The Ph.D. grant of Shian Guan was supported by the China Scholarship Council. The authors would like to thank Eric Lebraud, Sonia Buffière, Laetitia Etienne, and Denux Dominique for their assistance during XRD, SEM & TEM, ICP, and DSC measurements.

References

1. Cui, Y.; Ke, Y.; Liu, C.; Chen, Z.; Wang, N.; Zhang, L.; Zhou, Y.; Wang, S.; Gao, Y.; Long, Y. Thermochromic VO_2 for Energy-Efficient Smart Windows. *Joule.* 2018, *2*, 1707– 1746, DOI: 10.1016/j.joule.2018.06.018.
2. Liu, K.; Lee, S.; Yang, S.; Delaire, O.; Wu, J. Recent progresses on physics and applications of vanadium dioxide. *Mater. Today* 2018, *21*, 875– 896, DOI: 10.1016/j.mattod.2018.03.029.
3. Eyert, V. The metal-insulator transitions of VO_2: A band theoretical approach. *Ann. Phys. (Berlin, Ger.)* 2002, *11*, 650– 702, DOI: 10.1002/1521-3889(200210)11:9<650::AID-ANDP650>3.0.CO;2-K.
4. Belozerov, A. S.; Korotin, M. A.; Anisimov, V. I.; Poteryaev, A. I. Monoclinic M1 phase of VO_2: Mott-Hubbard versus band insulator. *Phys. Rev. B: Condens. Matter Mater. Phys.* 2012, *85*, 045109, DOI: 10.1103/PhysRevB.85.045109.
5. Berglund, C. N.; Guggenheim, H. J. Electronic Properties of VO, near the Semiconductor-Metal Transition. *Phys. Rev.* 1969, *185*, 1022–1033, DOI: 10.1103/PhysRev.185.1022.
6. Cui, Y.; Shi, S.; Chen, L.; Luo, H.; Gao, Y. Hydrogen-doping induced reduction in the phase transition temperature of VO_2: A first-principles study. *Phys. Chem. Chem. Phys.* 2015, *17*, 20998– 21004, DOI: 10.1039/C5CP03267A.
7. Cui, Y.; Wang, Y.; Liu, B.; Luo, H.; Gao, Y. First-principles study on the phase transition temperature of X-doped (X = Li, Na or K) VO_2. *RSC Adv.* 2016, *6*, 64394– 64399, DOI: 10.1039/C6RA10221B.
8. Zhang, J.; He, H.; Xie, Y.; Pan, B. Theoretical study on the tungsten-induced reduction of transition temperature and the degradation of optical properties for VO_2. *J. Chem. Phys.* 2013, *138*, 114705– 114710, DOI: 10.1063/1.4795431.
9. Zou, J.; Shi, H.; Su, X.; Feng, Q.; Liang, S. A simple method to prepare $V_{1-x}W_xO_2$ (x= 0, 0.01, 0.02, 0.03, 0.04, and 0.05) controllable phase transition temperature powder. *J. Alloys Compd.* 2017, *708*, 706– 712, DOI: 10.1016/j.jallcom.2017.03.081.
10. Zhou, J.; Xie, M.; Cui, A.; Zhou, B.; Jiang, K.; Shang, L.; Hu, Z.; Chu, J. Manipulating Behaviors from Heavy Tungsten Doping on Interband Electronic Transition and Orbital Structure Variation of Vanadium Dioxide Films. *ACS Appl. Mater. Interfaces* 2018, *10*, 30548– 30557, DOI: 10.1021/acsami.8b09909.
11. Chen, R.; Miao, L.; Liu, C.; Zhou, J.; Cheng, H.; Asaka, T.; Iwamoto, Y.; Tanemura, S. Shape-controlled synthesis and influence of W doping and oxygen nonstoichiometry on the phase transition of VO_2. *Sci. Rep.* 2015, *5*, 14087, DOI: 10.1038/srep14087.
12. Tan, X.; Yao, T.; Long, R.; Sun, Z.; Feng, Y.; Cheng, H.; Yuan, X.; Zhang, W.; Liu, Q.; Wu, C.; Xie, Y.; Wei, S. Unraveling Metal-insulator Transition Mechanism of VO_2 Triggered by Tungsten Doping. *Sci. Rep.* 2012, *2*, 466, DOI: 10.1038/srep00466.
13. Mai, L. Q.; Hu, B.; Hu, T.; Chen, W.; Gu, E. D. Electrical property of Mo-doped VO_2 nanowire array film by melting-quenching sol-gel method. *J. Phys. Chem. B* 2006, *110*, 19083– 19086, DOI: 10.1021/jp0642701.
14. Malarde, D.; Johnson, I. D.; Godfrey, I. J.; Powell, M. J.; Cibin, G.; Quesada-Cabrera, R.; Darr, J. A.; Carmalt, C. J.; Sankar, G.; Parkin, I. P.; Palgrave, R. G. Direct and continuous hydrothermal flow synthesis of thermochromic phase pure monoclinic VO_2 nanoparticles. *J. Mater. Chem. C* 2018, *6*, 11731– 11739, DOI: 10.1039/C8TC00859K.
15. Barron, S. C.; Gorham, J. M.; Patel, M. P.; Green, M. L. High-Throughput Measurements of Thermochromic Behavior in $V_{1-x}Nb_xO_2$ Combinatorial Thin Film Libraries. *ACS Comb. Sci.* 2014, *16*, 526– 534, DOI: 10.1021/co500064p.
16. Piccirillo, C.; Binions, R.; Parkin, I. P. Nb-Doped VO_2 Thin Films Prepared by Aerosol-Assisted Chemical Vapour. *Eur. J. Inorg. Chem.* 2007, *2007*, 4050– 4055, DOI: 10.1002/ejic.200700284.
17. Jorgenson, G. V.; Lee, J. C. Doped Vanadium Oxide for Optical Switching Films. *Sol. Energy Mater.* 1986, *14*, 205– 214, DOI: 10.1016/0165-1633(86)90047-X.
18. Batista, C.; Ribeiro, R. M.; Teixeira, V. Synthesis and Characterization of VO_2-Based Thermochromic Thin Films for Energy-Efficient Windows. *Nanoscale Res. Lett.* 2011, *6*, 301, DOI: 10.1186/1556-276X-6-301.
19. Rao, C. N. R.; Natarajan, M.; Subba Rao, G. V.; Loehman, R. E. Phase Transitions and Conductivity Anomalies in Solid Solutions of VO_2 with TiO_2, NbO_2, and MoO_2. *J. Phys. Chem. Solids* 1971, *32*, 1147– 1150, DOI: 10.1016/S0022-3697(71)80172-5.
20. Villeneuve, G.; Bordet, A.; Casalot, A.; Pouget, J. P.; Launois, H.; Lederer, P. Contribution to the Study of the Metal-Insulator Transition in the $V_{1-x}Nb_xO_2$ System: I-Crystallographic and Transport Properties. *J. Phys. Chem. Solids* 1972, *33*, 1953– 1959, DOI: 10.1016/S0022-3697(72)80494-3.

Shian Guan, Mélanie Souquet-Basiège, Olivier Toulemonde, Dominique Denux, Nicolas Penin, et al.. Toward room-temperature thermochromism of VO_2 by Nb doping : magnetic investigations. *Chemistry of Materials*, American Chemical Society, 2019, 31 (23), pp.9819-9830. ⟨10.1021/acs.chemmater.9b03906⟩. ⟨hal-02401952⟩

21. Guan, S.; Gaudon, M.; Souquet-Basiège, M.; Viraphong, O.; Penin, N.; Rougier, A. Carbon-reduction as an easy route for the synthesis of VO_2 (M1) and further Al, Ti doping. *Dalton. Trans.* 2019, *48*, 3080– 3089, DOI: 10.1039/C8DT04914A.
22. Mjejri, I.; Rougier, A.; Gaudon, M. Low-cost and facile synthesis of the vanadium oxides V_2O_3, VO_2, and V_2O_5 and their magnetic, thermochromic and electrochromic properties. *Inorg. Chem.* 2017, *56*, 1734– 1741, DOI: 10.1021/acs.inorgchem.6b02880.
23. Qi, J.; Ning, G.; Lin, Y. Synthesis, characterization, and thermodynamic parameters of vanadium dioxide. *Mater. Res. Bull.* 2008, *43*, 2300– 2307, DOI: 10.1016/j.materresbull.2007.08.016.
24. Son, J. H.; Wei, J.; Cobden, D.; Cao, G.; Xia, Y. Hydrothermal synthesis of monoclinic VO_2 micro- and nanocrystals in one step and their use in fabricating inverse opals. *Chem. Mater.* 2010, *22*, 3043, DOI: 10.1021/cm903727u.
25. Wu, C.; Dai, J.; Zhang, X.; Yang, J.; Qi, F.; Gao, C.; Xie, Y. Direct confined-space combustion forming monoclinic vanadium dioxides. *Angew. Chem., Int. Ed.* 2010, *49*, 134– 137, DOI: 10.1002/anie.200905227.
26. Quesada-Cabrera, R.; Powell, M. J.; Marchand, P.; Denis, C. J.; Maggio, F. D.; Darr, J. A.; Parkin, I. P. Scalable Production of Thermochromic Nb-Doped VO_2 Nanomaterials Using Continuous Hydrothermal Flow Synthesis. *J. Nanosci. Nanotechnol.* 2016, *16*, 10104– 10111, DOI: 10.1166/jnn.2016.12842.
27. Zhang, R.; Fu, Q. S.; Yin, C. Y.; Li, C. L.; Chen, X. H.; Qian, G. Y.; Lu, C. L.; Yuan, S. L.; Zhao, X. J.; Tao, H. Z. Understanding of metal-insulator transition in VO_2 based on experimental and theoretical investigations of magnetic features. *Sci. Rep.* 2018, *8*, 17093, DOI: 10.1038/s41598-018-35490-5.
28. Cavanna, E.; Segaud, J. P.; Livage, J. Optical Switching of Au-doped VO_2 sol-gel films. *Mater. Res. Bull.* 1999, *34*, 167– 177, DOI: 10.1016/S0025-5408(99)00017-3.
29. Mlyuka, N. R.; Niklasson, G. A.; Granqvist, C. G. Applied Physic Letters, Mg doping of thermochromic VO_2 films enhances the optical transmittance and decreases the metal-insulator transition temperature. *Appl. Phys. Lett.* 2009, *95*, 171909– 171911, DOI: 10.1063/1.3229949.
30. Ordonez-Miranda, J.; Ezzahri, Y.; Joulain, K.; Drevillon, J.; Alvarado-Gil, J. J. Modeling of the electrical conductivity, thermal conductivity, and specific heat capacity of VO_2. *Phys. Rev. B: Condens. Matter Mater. Phys.* 2018, *98*, 075144, DOI: 10.1103/PhysRevB.98.075144.
31. Kleinschmidt, P. Electrical conductivity-measurements on doped VO_2 single-crystals. *Phys. Lett. A* 1974, *47*, 205– 206, DOI: 10.1016/0375-9601(74)90009-7.
32. Gentle, A.; Smith, G. B. Dual metal-insulator and insulator-insulator switching in nanoscale and Al doped VO_2. *J. Phys. D: Appl. Phys.* 2008, *41*, 015402– 015406, DOI: 10.1088/0022-3727/41/1/015402.
33. Miiller, W.; Avdeev, M.; Zhou, Q.; Kennedy, B. J.; Sharma, N.; Kutteh, R.; Kearley, G. J.; Schmid, S.; Knight, K. S.; Blanchard, P. E.; Ling, C. D. Giant Magnetoelastic Effect at the Opening of a Spin-Gap in $Ba_3BiIr_2O_9$. *J. Am. Chem. Soc.* 2012, *134*, 3265– 3270, DOI: 10.1021/ja211517h.
34. Goodenough, J. B. Direct cation-cation interactions in several oxides. *Phys. Rev.* 1960, *117*, 1442– 1451, DOI: 10.1103/PhysRev.117.1442.
35. Popuri, S. R.; Artemenko, A.; Decourt, R.; Villesuzanne, A.; Pollet, M. Presence of Peierls pairing and absence of insulator-to-metal transition in VO_2 (A): a structure-property relationship study. *Phys. Chem. Chem. Phys.* 2017, *19*, 6601– 6609, DOI: 10.1039/C7CP00248C.
36. Wang, Z.-L.; Zhang, R.; Chen, X.-H.; Fu, Q.-S.; Li, C.-L.; Yuan, S.-L.; Zhao, X.-J.; Tao, H.-Z. Nb doping effect in VO_2 studied by investigations of magnetic behavior. *Ceram. Int.* 2018, *44*, 8623– 8627, DOI: 10.1016/j.ceramint.2018.02.079.
37. Kolodiazhnyi, T.; Wimbush, S. C. Spin-Singlet Small Bipolarons in Nb-Doped $BaTiO_3$. *Phys. Rev. Lett.* 2006, *96*, 246404– 246407, DOI: 10.1103/PhysRevLett.96.246404.
38. Pouget, J. P.; Lederer, P.; Schreiber, D. S.; Launois, H.; Wohlleben, D.; Casalot, A.; Villeneuve, G. Contribution to the study of the metal-insulator transition in the $V_{1-x}Nb_xO_2$ system-II magnetic properties. *J. Phys. Chem. Solids* 1972, *33*, 1961– 1967, DOI: 10.1016/S0022-3697(72)80495-5.